Finite volume model for the simulation of 1D unsteady river flow and water quality based on the WASP

Geovanny Gordillo, Mario Morales-Hernández and Pilar García-Navarro

ABSTRACT

In this work, a one-dimensional (1D) finite volume numerical model for the unsteady simulation of the flow hydrodynamics and water quality is developed. The water dynamics is formulated with the 1D shallow water equations, and the water quality evolution is described by the Water Quality Analysis Simulation Program (WASP) model, allowing us to interpret and predict the transport and fate of various biochemical substances along any river reach. This combined system is solved with an explicit finite volume scheme based on Roe's linearization for the advection component of both the flow and the solute transport equations. The proposed model is able to consider temporal variations in tributaries and abstractions occurring in the river basin. This feature is transcendent in order to predict the chemical composition of natural water bodies during winter and summer periods, leading to an improvement in the agreement between computed and observed water quality evolutions. The combined model has been evaluated using literature tests in a steady state and a real-field case of the Ebro river (Spain), characterized by a marked unsteady regime. In the real case, we found that the water temperature was very sensitive to both the solar radiation and the average air temperature, requiring a careful calibration of these parameters. The numerical results are also demonstrated to be reasonably accurate, conservative and robust in real-scale field cases, showing that the model is able to predict the evolution of quality parameters as well as hydrodynamic variables in complex scenarios.

Key words | finite volume method, one-dimensional, WASP, water quality

Geovanny Gordillo (corresponding author)
Mario Morales-Hernández
Pilar García-Navarro
Fluid Mechanics,
University of Zaragoza/LIFTEC-CSIC,
Zaragoza,
Spain
E-mail: ggordillo@unizar.es

INTRODUCTION

How do the kinetics process and hydraulics impact on water quality in a real environment? The answer to this question began in 1912 when the Royal Commission on Sewage Disposal put into practice the biochemical oxygen demand (BOD) and dissolved oxygen (DO) measurement and interpretation in natural environments. Since then, many works have been carried out in this field. As an example, Streeter & Phelps (1958) developed a seminal work on how to assess the impact of the discharge BOD on DO in a river system. After that, the use of mathematical models has become more and more important in DO modelling for streams and estuaries. Other works like O'Connor (1961) and Thomann (1963) observed that the BOD parameter can

be divided into carbonized and nitrified or that the BOD reduction can be carried out without oxygen consumption.

Another advance in terms of water quality came from the hand of the continuous progress of computers in order to improve the prediction of pollutant transport. This prediction is still a subject of interest at present, due to the conversion processes and coupling with hydrodynamics.

Based on the conversion processes, many models have emerged, such as QUAL (Brown & Barnwell 1987), Water Quality Analysis Simulation Program (WASP) (Ambrose et al. 1993) or RWQM1 (Reichert et al. 2001), that have been used to simulate and predict the detrimental effect of the discharge of organic waste on the oxygen concentration.

With respect to the coupling, some of the aforementioned quality models have been combined with 1D and two-dimensional (2D) hydrodynamic solvers such as MIKE11 (DHI 2009), HSPF (Ambrose *et al.* 1989) and HEC-RAS (Brunner 2010) to simulate the kinetic processes involving DO in lowland rivers. From this combination, numerous studies on modelling have been reported, but the WASP quality model has been the most widely used in several countries with different hydrodynamic models.

The WASP model was used to evaluate the parameter sensitivity in the lower course of the Saale river (Lindenschmidt 2006). It was also reported to obtain a longitudinal profile of DO and to quantify the shift of the water quality under low flow conditions (Huang *et al.* 2017). The WASP model has been considered to assess the effects of installing a new wastewater treatment plant for treating wastewater from a residential area of Malaysia (Lee *et al.* 2017). In Jian *et al.* (2014), a three-dimensional unstructured mesh ecological model was developed to investigate the algal bloom in the Xiangxi River. The pollution source with the WASP was also analysed by Yao *et al.* (2015) to evaluate the risk of point-wise pollution on a regional scale in the Taipu River.

These mathematical models have proved to be useful for analysing or predicting the fate and transport of contaminants in rivers in the context of steady flow. However, sometimes it is necessary to evaluate the water quality evolution in the presence of discharge variation. Therefore, the water quality model and the hydrodynamic model must be applied in a coupled way, i.e., solving both at the same time rather than assuming a steady-state flow model. In the context of unsteady flow, Cea *et al.* (2016) evaluated their freeware simulation tool (IberWQ), which computes the spatial and temporal evolution of several species, showing some of the 2D model's capabilities and limitations. This evaluation requires processes of the calibration of coefficients, for a later numerical validation with experimental data in more complex transport environments. Despite many contributions, no combined model provides all the required functionality. In other words, all models have different limitations and strengths that still need to be studied in more detail (Cox 2003; Kannel *et al.* 2011; Liangliang & Daoliang 2015). Some of these limitations refer to (a) that it is not possible to correlate the temporal variability of the flow with the quality parameters in different sites, (b) it is not possible to correlate the flow variability between the main river, its tributaries and discharges or (c) that it does not properly consider the seasonal or diurnal effects on quality.

In this framework, the main novelty of the present work is the development of a simulation model in 1D to predict the fate and transport of pollutants and hydrodynamic variables in unsteady river flow. The hydraulic modelling is based on the 1D shallow water equations written to consider realistic and irregular cross-sections.

For the quality module, the equations of the WASP, including the temperature, are used. In this water quality model, the variables considered belong to three groups: suspended solids removed from the river bottom, chemical compounds by anthropogenic activities (bacteria and virus due to human activities) and chemical compounds released by weathering processes. The interaction of these biochemical species generates quality indicators (such as BOD and DO) frequently measured in the natural water bodies. The most frequent state variables in a river water quality model are algae, nutrients (phosphorus cycle and nitrogen cycle) and DO. They have been included in the present work together with their specific biochemical processes. The formulation follows the model EUTRO, as included in the WASP5 simulation package, because it allows us to predict the kinetic processes more real (Ambrose *et al.* 1993).

A finite volume approximation has been used to solve the set of equations leading to the calculation of the evolution of flows, depths and all the water quality variables both in space and time. This approach is also a novelty since it allows us to predict the flow evolution under all flow regimes and the water quality variables in complex scenarios that consider both the temporal variability of the flow and the superficial changes. Previous works have reported the convenience of a careful formulation and discretization of these equations to deal with unsteady flow over a dry irregular bed (Burguete & Garcia-Navarro 2001; Murillo & Garcia-Navarro 2014). Furthermore, previous authors have indicated the necessity to implement a coupled discretization of the shallow water equations and the transport equations in order to avoid numerical difficulties. This idea was included in Burguete & Garcia-Navarro (2001); Murillo *et al.* (2009) for the 1D case and in Cea &

Vázquez-Cendón (2012) for the 2D case using the pure advection of a passive solute. In the present work, this has been extended to include a water quality model with the ambition to be able to deal with unsteady flow in complex and realistic river cross-sections.

The numerical method applied for the advective part is an explicit first-order Roe's scheme which has been previously proved robust and well behaved for this kind of problem (Burguete *et al.* 2008). The novelty is the dynamical coupling of the models and their simultaneous numerical resolution using a single finite volume scheme based on a global time stepping that dynamically controls the numerical stability of the solution either under steady or unsteady conditions. This is achieved as well as offering the possibility to involve all sorts of source terms in the equations (bed slope, cross-section changes, friction, heat flux and all the water quality kinetic terms). Furthermore, the numerical formulation ensures conservative solutions which are crucial when dealing with the transport processes in water quality simulations. The model is validated with theoretical cases, with well-known analytical solutions and with a real case of the Ebro river (Spain).

MATHEMATICAL MODELS FOR THE FREE SURFACE FLOW SIMULATION AND TRANSPORT OF SOLUTES

The fate and transport processes of contaminants are controlled by two factors: their reactivity and their hydrodynamic transport. The formulation of both models is next presented.

Hydraulic model

The 1D shallow water equations or Saint Venant equations allow us to describe the flow of water within reach of the river. These equations encompass the mass and momentum conservation. The systems of equations are expressed as follows:

$$\frac{\partial A}{\partial t} + \frac{\partial Q}{\partial x} = q$$
$$\frac{\partial Q}{\partial t} + \frac{\partial}{\partial x}\left(\frac{Q^2}{A} + gI_1\right) = g[I_2 + A(S_o - S_f)] \tag{1}$$

where A is the cross-section area, t is the time, Q is the discharge, x is the longitudinal distance, q is the lateral inflow per unit width, g is the acceleration due to gravity and S_o is the bed slope defined as $S_o = -\partial z/\partial x$ where z is the lowest bottom level in the cross-section. S_f is the friction slope expressed by means of semi-empirical Manning's law:

$$S_f = \frac{n_M^2 |Q|Q}{A^2 R_h^{4/3}} \tag{2}$$

where n_M^2 is the Gauckler–Manning coefficient and $R_h = A/P$ is the hydraulic radius, being P the wetted perimeter. I_1 is the hydrostatic pressure force term.

$$I_1 = \int_0^{h(x,t)} \sigma(x, \eta)d\eta \tag{3}$$

where h is the water depth, σ is the channel width (see Figure 1) and I_2 is the pressure force due to the longitudinal width variations:

$$I_2 = \int_0^{h(x,t)} (h - \eta)\frac{\partial \sigma(x, \eta)}{\partial x} d\eta \tag{4}$$

The above formulation is widely accepted as a good approximation for long reaches when considering sections of real rivers.
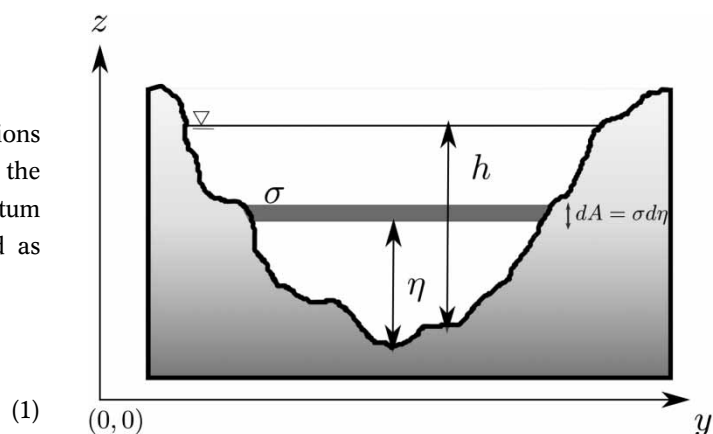
Figure 1 | Cross-section sketch and geometrical variables used in the model 1D.

Water quality model

A water quality model with source/sink terms in 1D can be mathematically represented by a system of advection equations, with reagent constituents, assuming a first-order decay reaction (the rate of loss of the substance is proportional to the concentration at any time). This equation can be written as follows:

$$\frac{\partial(A\phi_i)}{\partial t} + \frac{\partial(Q\phi_i)}{\partial x} = \pm AR_i \pm f_i \tag{5}$$

where ϕ_i is the section average concentration of each constituent, f_i is the load term that indicates external sources/sinks (point and non-point sources/sinks) in a water volume and R_i is the term used to represent the kinetic process responsible for the disappearance or formation of each constituent or chemical species i (reactivity).

The advective transport is a result of passive movement along with the flow. The diffusive transport caused by Brownian motion as well as turbulence is influenced by the fluid temperature and the size of the molecules. Also, this term will be affected by the slope, morphology and roughness. This means that it varies according to the direction of the flow. For this case, we assume that the dispersion coefficient is independent of any direction, so that the surface water body is homogeneous and isotropic. In order to compute this term, many empirical and analytical expressions exist in the literature (Chen *et al.* 2012; Wang *et al.* 2017).

In Equation (5), the term R_i governs the permanence of pollutants in a body of water depending on the nature of the compound. Most chemicals undergo biological or chemical decay. For this study, the solutes are non-conservative, that is, the pollutants can chemically or biologically decay. These fate and decay processes include volatilization, hydrolysis, photolysis and biodegradation and have been addressed and characterized by Thomann & Mueller (1987); Chapra (2008); Ji (2017), among others.

The list of the kinetic processes considered is summarized in Table 1. A detailed description of each decay rate for each process of Table 1 is given in Appendix Notation in Supplementary Materials.

The formation or disappearance of each constituent in the water column, due to its inherent process, will be discussed in detail in the following subsections.

Dissolved oxygen

The DO (ϕ_6) is one of the most important parameters of water quality, because it is a basic requirement for a healthy aquatic ecosystem. The DO concentration in a stream can change through an exchange with the atmosphere (coefficient k_a) and the growth of algae (photosynthesis).

Table 1 | Processes and variables for eutrophication modelling

Ammonia nitrogen (ϕ_1): $R_1 = k_{1D}a_{nc}(1-f_{on})\phi_4 + k_{71}(T)\left(\dfrac{\phi_4}{k_{mPc}+\phi_4}\right)\phi_7 - k_{12}(T)\left(\dfrac{\phi_6}{k_{NIT}+\phi_6}\right)\phi_1 - G_{p1}a_{nc}P_{NH_3}\phi_4$

Nitrate nitrogen (ϕ_2): $R_2 = k_{12}(T)\left(\dfrac{\phi_6}{k_{NIT}+\phi_6}\right)\phi_1 - G_{p1}a_{nc}(1-P_{NH_3})\phi_4 - k_{2D}(T)\left(\dfrac{k_{NO_3}}{k_{NO_3}+\phi_6}\right)\phi_2$

Dissolved inorganic phosphorus (ϕ_3): $R_3 = k_{1D}a_{pc}(1-f_{op})\phi_4 + k_{83}(T)\left(\dfrac{\phi_4}{k_{mPc}+\phi_4}\right)\phi_8 - G_{p1}a_{pc}\phi_4$

Phytoplankton (ϕ_4): $R_4 = \left(G_{p1} - (k_{1D}+k_{1R}(T)) - \dfrac{V_{s4}}{h}\right)\phi_4$

CBOD (ϕ_5): $R_5 = a_{oc}k_{1D}\phi_4 - k_d(T)\left(\dfrac{\phi_6}{k_{BOD}+\phi_6}\right)\phi_5 - \dfrac{V_{s3}(1-f_{d5})}{h}\phi_5 - \dfrac{5}{4}\dfrac{32}{14}k_{2D}(T)\left(\dfrac{K_{NO_3}}{K_{NO_3}+\phi_6}\right)\phi_2$

DO (ϕ_6): $R_6 = k_a(T)(\phi_{sat}-\phi_6) - k_d(T)\left(\dfrac{\phi_6}{k_{BOD}+\phi_6}\right)\phi_5 - \dfrac{64}{14}k_{12}(T)\left(\dfrac{\phi_6}{k_{NIT}+\phi_6}\right)\phi_1 - \dfrac{SOD}{h}(T) + G_{p1}\left(\dfrac{32}{12}+\dfrac{48}{14}\dfrac{14}{12}(1-P_{NH_3})\right)\phi_4 - \dfrac{32}{12}k_{1R}(T)\phi_4$

ON (ϕ_7): $R_7 = k_{1D}a_{nc}f_{on}\phi_4 + a_{nc}k_{1R}(T)\phi_4 - k_{71}(T)\left(\dfrac{\phi_4}{k_{mPc}+\phi_4}\right)\phi_7 - \dfrac{V_{s3}(1-f_{d7})}{h}\phi_7$

OP (ϕ_8): $R_8 = k_{1D}a_{pc}f_{op}\phi_4 + a_{pc}k_{1R}(T)\phi_4 - k_{83}(T)\left(\dfrac{\phi_4}{k_{mPc}+\phi_4}\right)\phi_8 - \dfrac{V_{s3}(1-f_{d8})}{h}\phi_8$

However, its depletion is due to the oxidation of organic carbon (affected by coefficient k_d), nitrification (k_{12}), the death of algae (respiration k_{1R}) and the sediment oxygen demand (SOD), defined as the rate of DO required for the oxidation of organic matter in benthic sediments. The DO concentration frequently oscillates in the water column, but its oscillation is higher when it arises from the human activity. The complete process that includes all these gains and losses of DO in the water column can be expressed as R_6.

Carbonaceous BOD

The carbonaceous BOD (CBOD; ϕ_5) is the concentration of organic material present in the water body. This process (R_5) includes the effects of sedimentation, oxidation (k_d) and denitrification (k_{2D}). The principal sources of CBOD are man-made sources, algal death (k_{1d}) and natural runoff. There is a mutual interaction between the CBOD and the DO components, so that, in particular, the DO level will decrease when the injection of CBOD is continuous in time, causing an oxygen deficit.

Phytoplankton

The quality of a body of water can be affected by the presence of phytoplankton (ϕ_4). This population can be accelerated by the addition of nutrients (nitrogen and phosphorus), either by human activities or natural processes. The excess of nutrients provides more population growth. This uncontrolled growth is commonly referred to as eutrophication. When this population becomes large, it may cause diurnal variations in DO that can be fatal to fish life. Also, the presence of phytoplankton can cause water taste and odour problems.

The model considers two of the three primary dependent systems: the phytoplankton population and the nutrient system. The external environment variables that affect those systems are temperature, advective flow and solar radiation. The classical approach is to assume that these effects are multiplicative. Thereby, the increase of phytoplankton in rivers and streams is due to the availability of nutrients and solar energy, while its reduction occurs primarily through respiration. A simplified representation of this process is given by R_4.

Nitrogenous BOD (NBOD)

Nitrogen can be found in five major forms in aquatic environments: organic nitrogen (ON), ammonia (NH_3), nitrite (NO_2^-), nitrate (NO_3^-) and dissolved nitrogen gas (N_2). The sequential processes of nitrogen compounds transforming ON to NH_3, then to NO_2^- and finally to NO_3^-.

The ON (ϕ_7) originally present in water is partially transformed into NH_3 and partially settles on the bottom; meanwhile, the increase of ON is due to phytoplankton death. The ON kinetic equation describing these processes is expressed as R_7, involving (k_{71}).

NH_3 (ϕ_1) is one of the intermediate compounds formed during biological metabolism and, together with ON, is considered as an indicator of recent pollution. The ammonia concentration is increased by the change of ON to NH_3 due to mineralization and the production of nitrogen due to phytoplankton death and respiration. At the same time, its concentration is reduced by the uptake for phytoplankton growth and the change of NH_3 to NO_3^- due to nitrification. The corresponding kinetic process for this state variable is R_1.

NO_3^- (ϕ_2), the end product of nitrification, represents the sum of NO_2^- and NO_3^- (the amount of NO_2^- present in natural waters is usually very small). Its reduction is due to the growth of phytoplankton and the denitrification process (k_{2D}); meanwhile, its rise is generated by the nitrification process (k_{12}). Therefore, the total nitrate concentration can be expressed as R_2.

Phosphorus (OP, PO₃)

To model the phosphorus cycle, two single kinetic equations are taken into account: organic phosphorus (OP) (ϕ_8) and inorganic phosphorus PO_3^- (ϕ_3).

The production of OP is caused by phytoplankton death and respiration. Conversely, the loss of OP is due to mineralization and the settling process (R_8). The kinetics of PO_3^- is affected by the uptake for phytoplankton growth. However, the production of phosphorus is caused by phytoplankton death, respiration and mineralization. Hence, the mathematical equation for PO_3^- can be expressed as R_3.

All the kinetic equations that describe the increase or decrease of state variables in time as well as all the

coefficients controlling the rate of the processes are summarized in Tables 1 and 2.

Temperature

The integrity of all the processes can be largely affected by the river temperature. High or low water temperatures generate a potential risk for aquatic biota, biological and chemical reactions. Also, the rate coefficients of most reactions in natural waters are affected by the temperature. In the present work, some of the k_b biodegradation process coefficients have been made dependent on the temperature with reference to the rate at 20 °C (Ji 2017) as follows:

$$k_b(T) = k_b(20)\theta_R^{T-20} \tag{6}$$

where T is the temperature in degrees Celsius, k_b is the biodegradation rate and θ_R is a temperature correction factor for every process. According to Chapra (2008), the correction factor is bounded by $1.01 < \theta_R < 1.1$ for most steady processes.

In this study, following Edinger *et al.* (1968), a temperature transport model has been included assuming it as a scalar variable whose evolution can be formulated following also an advection–reaction equation. The total heat budget for a water body includes the effects of water depth, velocity and atmospheric conditions. For that purpose, it is useful to estimate the daily average stream temperature based on climate conditions (Gu & Li 2002; Herb & Stefan 2011).

Table 2 | Additional equations for eutrophication modeling

Reaeration coefficient of oxygen (k_a): $k_a = 3.9\dfrac{u^{1/2}}{h^{3/2}}$

Saturation oxygen (ϕ_{sat}): $\phi_{sat} = 0.0035T^2 - 0.3369T + 14.407$

Preference for ammonia term (P_{NH_3}):

$$P_{NH_3} = \left(\frac{\phi_2}{(k_{mN} + \phi_1)(k_{mN} + \phi_2)}\right)\phi_1 + \left(\frac{k_{mN}}{(\phi_1 + \phi_2)(k_{mN} + \phi_2)}\right)\phi_1$$

Phytoplankton growth rate (G_{p1}): $G_{p1} = K_{1c}X_{RT}X_{RI}X_{RN}$

Phytoplankton temperature adjustment: $X_{RT} = \theta_{1C}^{T-20}$

Phytoplankton light limitation (X_{RI}):

$X_{RI} = \dfrac{e}{K_E h}f_l\left[\exp\left\{-\dfrac{I_A}{I_S}\exp(-K_E h)\right\} - \exp\left(\dfrac{I_A}{I_S}\right)\right]$

Phytoplankton nutrient limitation (X_{RN}):

$X_{RN} = \min\left(\dfrac{\phi_1 + \phi_2}{k_{mN} + \phi_1 + \phi_2}, \dfrac{\phi_3}{k_{mP} + \phi_3}\right)$

The unsteady heat equation for a given water body in 1D, including cross-section and discharge variations, is expressed as follows:

$$\frac{\partial(AT)}{\partial t} + \frac{\partial(QT)}{\partial x} = \frac{AH_f}{\rho c_p h} \tag{7}$$

where T is the cross-sectional average water temperature, ρ is the water density, c_p is the heat capacity of water and H_f is the net heat input/output. The net rate of heat combining all weather variables is expressed as follows:

$$H_f = H_h(T_e - T) \tag{8}$$

where T_e is the equilibrium river temperature, representing the effects of meteorological conditions. Water would reach this temperature if all meteorological conditions were constant in time. The equilibrium temperature is approximated by:

$$T_e = T_d + \frac{R}{H_h} \tag{9}$$

where R is the net solar radiation and T_d is the dew point temperature. Edinger *et al.* (1968) showed that the exchange coefficient may be determined from empirical formulae listed in Table 3. The H_h term is an overall heat exchange coefficient which is a function of the water temperature and the wind speed.

The heat flux on the interface of the water column and the sediment bed also changes the water temperature, but

Table 3 | Empirical formulae for computing H_h

Parameter or coefficient	Expression
Heat exchange coefficient, H_h	$H_h = 4.5 + 0.05T + \beta f(U_w) + 0.47f(U_w)$
Wind function, $f(U_w)$	$f(U_w) = 9.2 + 0.46U_w^2$
Coefficient, β	$\beta = 0.35 + 0.015T_v + 0.0012T_v^2$
Average air temperature, T_v	$T_v = (T + T_d)/2$
Dew point temperature, T_d	$T_d = 237.3[T_a* + \ln(r_h)]/[17.27 - \ln(r_h) - T_a*]$
	$T_a* = 17.27T_a/(237.3 + T_a)$

this exchange with the sediment is much smaller than the surface exchange; hence it is neglected.

The temporal and spatial distribution of all the water quality constituents, temperature, water depth and discharge can be obtained by solving the problem from the initial conditions, assuming that boundary conditions and kinetic parameters are known.

NUMERICAL SCHEME

An explicit first-order upwind scheme has been used to solve the flow Equations (1) and the advective part of (5). It has been used, because it allows us to have greater control of the numerical stability when dealing with equations where source terms are as relevant as flux terms (Murillo & García-Navarro 2010). The balance between flows and source terms is accurate, therefore ensuring conservative solutions both in unsteady state and when approaching the steady state. In this way, no extra corrections are made, such as the hydrostatic reconstruction (Audusse *et al.* 2004). The formulation is written in a finite volume form, so that it can easily be extended to two dimensions and/or high-order schemes (Navas-Montilla & Murillo 2018).

In order to obtain a finite volume numerical solution of the hyperbolic nonlinear system of equations presented in the previous section, they are written as follows:

$$\frac{\partial \mathbf{U}(x,t)}{\partial t} + \frac{d\mathbf{F}(x,t)}{dx} = \mathbf{H}(x,\mathbf{U}) \tag{10}$$

with

$$\mathbf{U} = \begin{pmatrix} A \\ Q \end{pmatrix}, \quad \mathbf{F} = \begin{pmatrix} Q \\ \frac{Q^2}{A} + gI_1 \end{pmatrix} \quad \mathbf{H} = \begin{pmatrix} q \\ g[I_2 + A(S_0 - S_f)] \end{pmatrix} \tag{11}$$

where $\mathbf{U} = \mathbf{U}(x,t)$ is the vector of conserved variables, $\mathbf{F} = \mathbf{F}(x,t)$ their fluxes and $\mathbf{H} = \mathbf{H}(x,\mathbf{U})$ the source terms.

The system (10) can also be written in a quasi-conservative form as follows:

$$\frac{\partial \mathbf{U}(x,t)}{\partial t} + \mathbf{J}\frac{\partial \mathbf{U}(x,t)}{\partial x} = \mathbf{H}'(x,\mathbf{U}) \tag{12}$$

where $\mathbf{H}'(x,\mathbf{U})$ is the vector related with the sources and $\mathbf{J} = \dfrac{d\mathbf{F}}{dx}$ is the Jacobian matrix. This Jacobian matrix can be characterized by a set of approximate eigenvalues ($\lambda^1 = u - c, \lambda^2 = u + c$) and eigenvectors $\mathbf{e}^1$, $\mathbf{e}^2$ being $u = Q/A$ the average water velocity and c the small surface waves celerity. They are useful to decouple the system by means of the diagonalized Jacobian $\mathbf{\Lambda} = \mathbf{P}^{-1}\mathbf{J}\mathbf{P}$, where:

$$\mathbf{P} = \begin{pmatrix} 1 & 1 \\ \lambda^1 & \lambda^2 \end{pmatrix}, \quad \mathbf{\Lambda} = \begin{pmatrix} \lambda^1 & 0 \\ 0 & \lambda^2 \end{pmatrix}, \quad \mathbf{e}^k = \begin{pmatrix} 1 \\ \lambda^k \end{pmatrix} \tag{13}$$

System (12) can be discretized in a regular mesh of size Δx by means of a first-order explicit upwind scheme. Roe's linearization (Morales-Hernández *et al.* 2012) allows us to express the differences in the conserved variables and in the source terms across the grid edges $j + 1/2$ between cells j and $j + 1$ as a sum of waves:

$$\delta\mathbf{U}_{j+1/2} = \mathbf{U}_{j+1} - \mathbf{U}_j = \sum_{m=1}^{2} (\tilde{\alpha}^m \tilde{\mathbf{e}}^m)_{j+1/2}$$

$$(\tilde{\mathbf{H}}' \Delta x)_{(j+1/2)} = \sum_{m=1}^{2} (\tilde{\beta}^m \tilde{\mathbf{e}}^m)_{j+1/2} \tag{14}$$

with

$$\tilde{\alpha}_1 = \frac{\tilde{\lambda}_2 \delta A - \delta Q}{2\tilde{c}} \quad \tilde{\alpha}_2 = \frac{-\tilde{\lambda}_1 \delta A + \delta Q}{2\tilde{c}} \quad \tilde{u} = \frac{\sqrt{A_j}u_i + \sqrt{A_{j+1}}u_{j+1}}{\sqrt{A_j} + \sqrt{A_{j+1}}}$$

$$\tilde{c} = \sqrt{g\frac{A_j + A_{j+1}}{B_j + B_{j+1}}} \quad \tilde{\beta}_1 = -\frac{1}{2\tilde{c}}\left\{ g\tilde{A}\left[(\tilde{S}_0 - \tilde{S}_f)\Delta x - \delta h + \frac{1}{\tilde{B}}\delta A \right] \right\} \tag{15}$$

with $\tilde{A} = \frac{1}{2}(A_j + A_{j+1})$ and $\tilde{B} = \frac{1}{2}(B_j + B_{j+1})$, and $\tilde{S}_0$ and $\tilde{S}_f$ are discretized using the technique of Murillo & García-Navarro (2012). Therefore, the numerical scheme for updating at all computational cells j is formulated as follows (Murillo & García-Navarro 2010):

$$\mathbf{U}_j^{n+1} = \mathbf{U}_j^n - \frac{\Delta t}{\Delta x}\left[\left(\sum_m \tilde{\lambda}^+ \tilde{\gamma}\tilde{e} \right)_{j-1/2}^m + \left(\sum_m \tilde{\lambda}^- \tilde{\gamma}\tilde{e} \right)_{j+1/2}^m \right]^n \tag{16}$$

being $\tilde{\gamma}_{j+1/2}^m = \left(\tilde{\alpha} - \dfrac{\tilde{\beta}}{\tilde{\lambda}} \right)_{j+1/2}^m$, Δt the time-step size, super-script n stands for the discrete-time level and superscript m corresponds to the eigenvalues counter.

For the numerical solution of the water quality transport (Equation (5)), three steps have been considered: advective part, diffusive part and reactive part. For the sake of clarity, the transport of only one of the solutes is presented; therefore, the sub-index i labelling the different water quality components is dropped in this section.

Advective part

$$\frac{\partial(A\phi)}{\partial t} + \frac{\partial(Q\phi)}{\partial x} = 0 \tag{17}$$

The numerical solution of the advective part of the transport equation of a substance can be obtained under an explicit finite volume method following Morales-Hernández *et al.* (2018). The scheme to update the concentration at all cells j becomes:

$$(A\phi)_{j*} = (A\phi)_j^n - \frac{\Delta t}{\Delta x}[(q\phi)_{j+1/2}^{\downarrow} - (q\phi)_{j-1/2}^{\downarrow}]^n \tag{18}$$

where $q^{\downarrow}$ is defined to decouple the advective solute transport completely from the hydrodynamic system in a conservative way (Morales-Hernández *et al.* 2018):

$$q_{j+1/2}^{\downarrow} = Q_j + \sum_{2}^{m=1} (\tilde{\lambda}^- \tilde{\gamma} \tilde{\mathbf{e}}^1)_{j+1/2}^m \tag{19}$$

Conversely,

$$\phi_{j+1/2}^{\downarrow} = \begin{cases} \phi_j & \text{if } q_{j+1/2}^{\downarrow} > 0 \\ \phi_{j+1} & \text{if } q_{j+1/2}^{\downarrow} < 0 \end{cases} \tag{20}$$

The explicit nature of the scheme implies a restriction in the time-step size Δt. This time step is governed by the Courant–Freidrichs–Lewy (CFL) condition, defined as follows (Hirsch 2007):

$$\Delta t = \text{CFL} \min_{j,m} \left(\frac{\Delta x}{|\tilde{\lambda}^m|_j^n} \right), \qquad \text{CFL} \leq 1 \tag{21}$$

It is worth noting that this global step is dynamically computed and controls the stability of the coupled system.

Reactive part

To solve the reactive part of each constituent, a simple Pertersen matrix is constructed to take into an account all the processes (see Table 1):

$$\frac{\partial(A\phi)}{\partial t} = AR \tag{22}$$

$$(A\phi)_j = (A\phi)_j + \Delta t(AR)_j \tag{23}$$

This matrix incorporates the processes (rows) and variables of the state (columns) of the eutrophication model, and the elements within the matrix include the coefficients that establish the mass relationships between the components in the individual processes (Reichert *et al.* 2001). The configuration of this matrix allows an easy and fast recognition of the fate of each state variable. The term R is obtained by adding the products of the stoichiometric coefficients and the process rate for each component i that is considered.

NUMERICAL RESULTS

Once the theoretical development of the equations has been presented, it is crucial to pass to the stage of testing or tuning the model. Such testing should include a consistent set of contaminant transport scenarios.

On the one hand, there exist analytical solutions to 1D advective–dispersive transport that represent basic benchmark tests for the numerical schemes, providing sensitivity analyses to the numerical parameters. They have already been validated with the proposed scheme (Gordillo *et al.* 2018). Conversely, it is important to evaluate the well-balanced property of the method for the advective transport in complex situations. Finally, the evaluation of the model results with field data, when available, is also indispensable to achieve a calibrated, verified and validated model.

Case 1

A dambreak flows with advective solute transport in a channel of variable geometry. The formulation here presented is able to provide stable and accurate results for both steady and unsteady flows even in the presence of complex channel geometry, including discontinuous initial conditions. The proposed case presents the results obtained with the coupled scheme for the advective transport of a passive solute. The test used is a dambreak in a 100 m long frictionless channel with the variable width. The width of the channel is 5 m from $x = 0$ to $x = 50$ m and 30 m from $x = 55$ to $x = 100$ m. There is also a bottom discontinuity located at the same point of dam, the ratio is 2:0. Discontinuous initial conditions are assumed both in the water depth, with a ratio of initial heights of 4:1, and in the initial solute concentration, with a ratio of 1:0. The dam or gate is located at $x = 30$ m. The water is assumed to be initially at rest. The initial discontinuity is equivalent to a sudden and total gate opening. No diffusion or reaction terms are included in order to evaluate the ability of the scheme to simulate the advective transport free from oscillations in this complex test case. The case used a $\Delta x = 0.5$ m and CFL $= 1$ for the entire simulation.

Figure 2(a) represents the initial condition, and Figure 2(b) shows the numerical solution for the longitudinal water depth profile at several times after the dam removal. Figure 3 shows the longitudinal profile of the concentration at the same times. The discontinuity of concentration advances from 30 m from 1 to 0 g/m³ without oscillations. The advection speed is altered when the concentration front enters the channel widening zone becoming slower compared to the upstream advection speed. The proposed scheme is robust and reliable giving good approaches to sharply unsteady scenarios.

An additional case is proposed based on the geometric and hydraulic conditions of Case 1. For this scenario, the initial solute concentration is assumed uniform over the full domain with a value of 1 g/m³. The objective of this case is

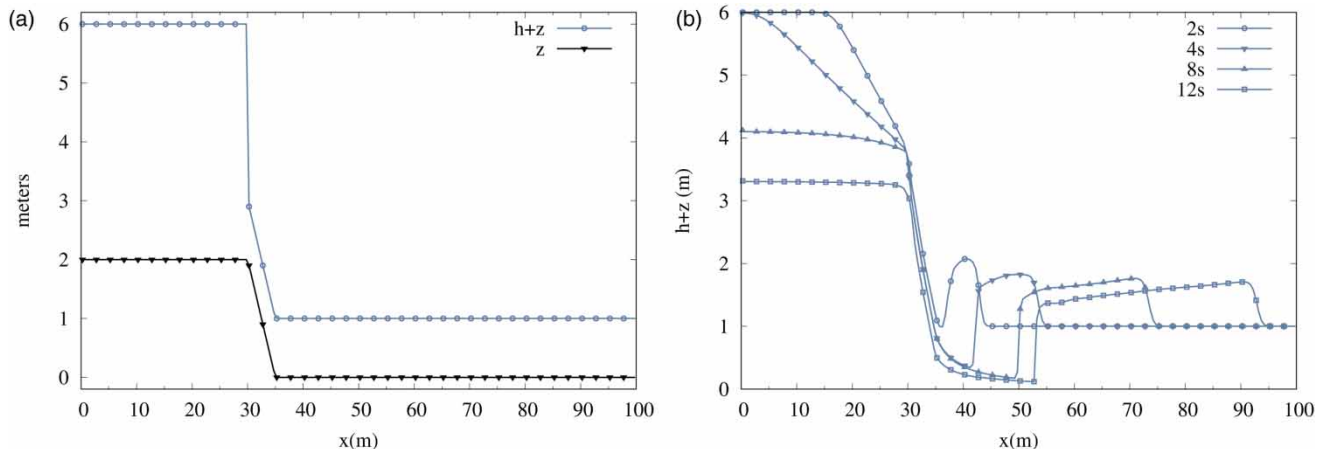**Figure 3** │ Longitudinal concentration profile with initial discontinuity 1:0.

Figure 2 │ Case 1. Longitudinal profiles. (a) Initial longitudinal profiles of both the bottom and the depth (b) Longitudinal water depth profile at several times.
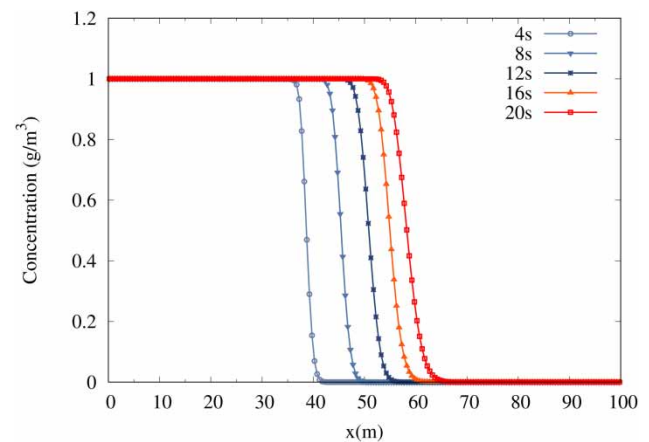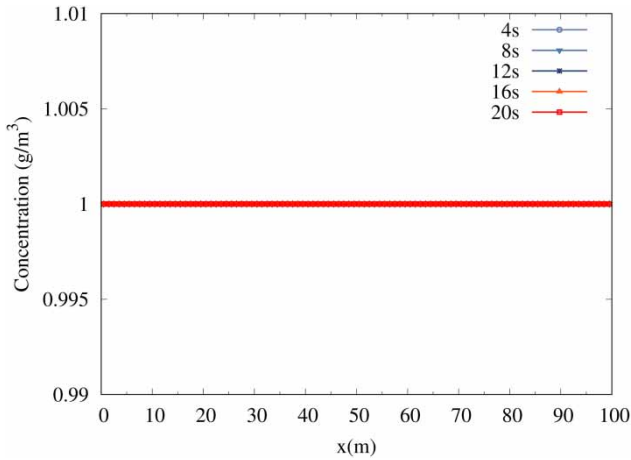
Figure 4 | Longitudinal concentration profile with an uniform initial condition.

to show that the concentration profile remains unchanged during the simulation despite the severe flow conditions. Figure 4 shows the longitudinal profile of concentration without discontinuity. As the unsteady flow develops, the passive solute maintains the initial concentration in the whole domain, verifying the proposed numerical properties again.

Case 2

The model is now evaluated with two state variables (CBOD and DO) and two-point sources. The example consists of observing the influence of point discharges in a mainstream over the DO.

A trapezoidal channel 110 km long with bottom width 10 m is assumed. The bottom slope is $S_0 = 0.0002$ from 0 to 60 km and $S_0 = 0.00018$ from 60 km onwards. The roughness coefficient $n_M = 0.035$ is considered in this case. A sewage treatment plant located at $x = 10$ km releases a flow $q_1 = 0.463$ m^3/s with 200 g/m^3 of CBOD and 2 g/m^3 of DO. The mainstream flow in the channel is $Q = 5.785$ m^3/s, with an initial CBOD concentration of 2 g/m^3 and an initial DO concentration of 7.5 g/m^3. There is a second point source (tributary) at 50 km downstream where a treatment plant discharges a flow $q_2 = 1.157$ m^3/s conveying 5 g/m^3 of CBOD and 9 g/m^3 of DO.

The decomposition process R_5 of the CBOD is $k_d = 0.5$d^{-1}.

Even though the temperature evolution is not simulated in this steady flow case, all the coefficients have been calculated as a function of the temperature using Equation (6).

Both point sources have different entry temperatures: the flow of the main stream has a temperature of 20 °C; however, that of the plant and tributary are 28 and 15 °C, respectively. The SOD often plays a significant role in affecting the DO concentration. Therefore, it is considered as something crucial in the process. Figure 5 shows this effect in the reach from $x = 10$ to $x = 30$ km where SOD = 5 5 g m^{-2}d^{-1}. To see the case in detail, the reader can consult (Chapra 2008, p. 493).

The longitudinal profiles in Figure 5 show the concentrations of DO and CBOD obtained with the proposed model for the steady state. The solutions presented are very similar in comparison to the QUAL2E output. According to the DO kinetic equation described previously, the concentration falls to 4 4 g/m^3 approximately, due to the amount of CBOD present and the SOD process in the 30 km reach. Also, the temperature influences the DO concentration through the dependence of the different reaction speeds due to the increase in metabolic speeds of aquatic life.

Although the example is simple, it is useful to show the potential application of the model to assess the impact of point sources. The approach for this kind of scenario is satisfactory, encouraging the extension to a real case for water utility managers.

Case 3

To continue the evaluation, the model now also incorporates the nitrogen cycle. Therefore, the state variables taken
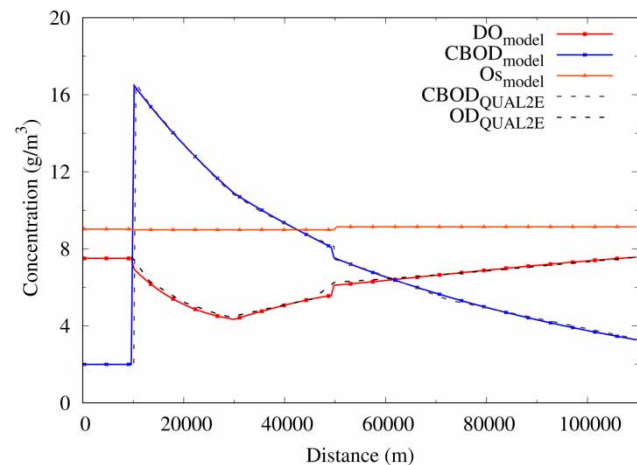
Figure 5 | Case 2. Concentration profiles of CBOD, oxygen saturation and DO with the proposed model vs. QUAL2E model.

into account for this case are DO, CBOD, $NH_3 - N$ and $NO_2 + NO_3 - N$. In the same way, as in Case 2, the main interest is focused on the variation in the concentration of DO following a point discharge. This case is based on a problem from Thomann & Mueller (1987) where the existence of field data is reported. All the data of the hydraulics characteristics of the channel and of the source are summarized in Table 4.

The predictions of the state variables for nitrogen are compared with the reported field data. The results are shown in Figure 6. The evolution of all the modelled solutes along the reach reproduces correctly the observed in-stream concentrations in Thomann & Mueller (1987).

As in the previous cases, the kinetic coefficients for organic matter degradation and nitrification were constant during all the simulation, but including the correction of these rates with the average flow temperature.

Case 4

The eutrophication in rivers and streams owing to the excessive discharge of nutrients, such as nitrogen and phosphorus, is the main objective of this test case. The focus is put on the predictive character of the model, in order to control the growth of aquatic plants in surface water body.

According to the description in Chapra (2008, p. 653), the kinetics of the nitrogen and phosphorus are incorporated in order to analyse the impact of nutrient-rich discharges on the phytoplankton. The participation of these new processes implies that other kinetics, such as CBOD, are modified to account for the effects of nitrification and plant growth/respiration.

Besides the changes in some kinetic processes, it is necessary to include the effect of solar radiation, because, in the natural environment, the light intensity to which the aquatic plants are exposed is not uniform (Di Toro *et al.* 1971). The empirical equation that determines this relation is given in Table 2. Another factor of this test case is the nutrient limitation at all times.

The heat balance Equation (7) was therefore included in this example in order to be able to follow the spatial and temporal evolution of the water temperature as a consequence of the changes in radiation and atmospheric conditions.

All the parameters for the nutrient/plant interactions in this test case and some others already mentioned have been extracted from the example nutrients and algae in QUAL2E (Chapra 2008). The results are displayed in Figures 7 and 8. In Figure 7, the water temperature profiles obtained from our model and the QUAL2E model are plotted, while that in Figure 8, the profiles of DO and saturation oxygen (ϕ_{sat}) are displayed. These profiles have been obtained after convergence to the steady state of the full set of transport equations involving the state variables, such as ON, NH_3, NO_3, NO_2, OP, PO_3^-, CBOD, Al and temperature T.

The results show that the interaction of all the processes leads to a decrease in the oxygen downstream, causing hypoxic conditions at $x = 30$ km. In this condition of DO levels (not very far from reality), it is likely that aquatic life is put under stress, so that foul odours, tastes and undesired colours might be produced if the low DO conditions are maintained for a prolonged period of time.

This test case is useful to stress the importance of considering the actual temperature of lateral streams acting as tributary sources of contaminant as they can alter not only the temperature of the mainstream but also the distribution and concentration of other water quality components.

Table 4 | Case 3. Parameters of the quality of the mainstream and the water treatment plant

Term	Unit	Value
Length	m	50,000
Width	m	30.5
Temperature	°C	25
$Q_{mainstream}$	m^3/s	2.832
$CBOD_{mainstream}$	g/m^3	2
$DO_{mainstream}$	g/m^3	8.3
$NH_3 - N_{mainstream}$	g/m^3	0.2
$NO_3 - N_{mainstream}$	g/m^3	0.5
$k_{d,mainstream}$	d^{-1}	0.3
$k_{12,mainstream}$	d^{-1}	0.15
$k_{2D,mainstream}$	d^{-1}	0.22
Q_{WWTP}	m^3/s	0.328
$CBOD_{WWTP}$	g/m^3	80
DO_{WWTP}	g/m^3	8.3
$NH_3 - N_{WWTP}$	g/m^3	15
$NO_3 - N_{WWTP}$	g/m^3	0.5
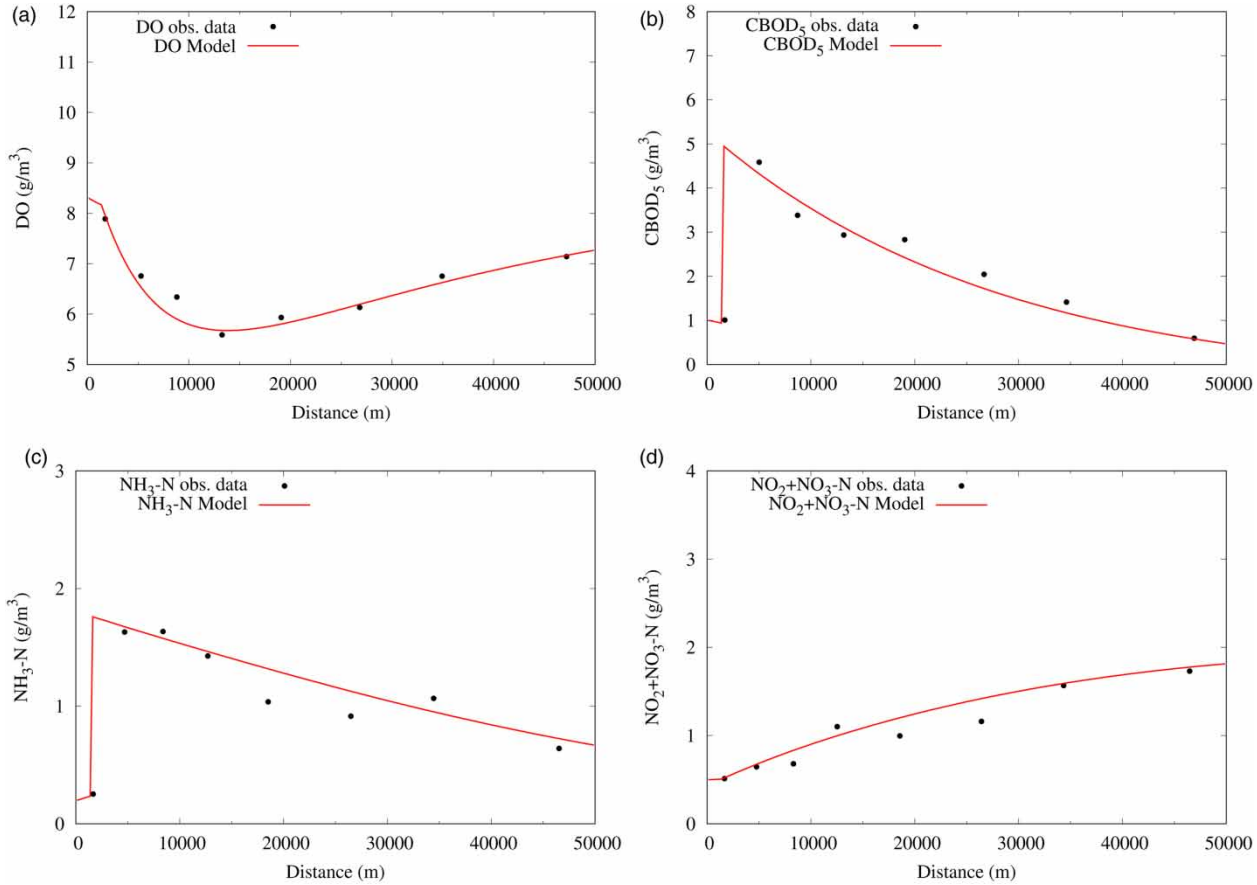
Figure 6 │ Case 3. Comparison of longitudinal concentration profiles of the nitrogen cycle in both the model and observed data. (a) Concentration profiles of DO (b) Concentration profiles of $CBOD_5$ (c) Concentration profiles of $NH_3 - N$ (d) Concentration profiles of $NO_2 + NO_3 - N$
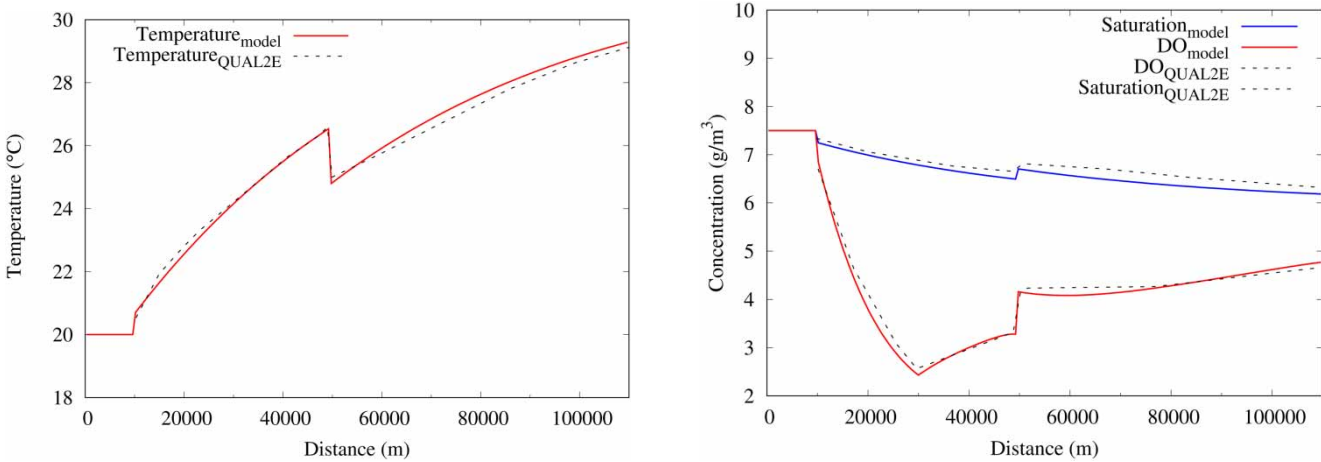
Figure 7 │ Case 4. Comparison of longitudinal profiles of the water temperature with nutrients in both the model and the QUAL2E output.

Figure 8 │ Case 4. Comparison of longitudinal profiles of DO and saturation oxygen with nutrients in both the model and the QUAL2E output.

Case 5

To assess the applicability of the proposed water quality model to a real case, the unsteady flow in a reach of the Ebro river (Spain) is next considered.

The Ebro river is the largest and longest river in Spain and has a total length of 930 km. Only the reach Alagón-Zaragoza with 44 km was considered in this example (Figure 9).

The period of validation of the model was from 3 July 2006 to 21 July 2006, and the data series for the flow rate and depth were provided by the Ebro Basin Water Authority (CHE). This public body has a fundamental work in terms of the hydrological planning, the quality of the waters, the control of the discharges, the environmental improvement and the execution of the fundamental works for the development of the territory.

The meteorological variables, such as air temperature, specific humidity and radiation, were collected from the database of the Aragonese Society of Agro-environmental Management (SARGA), which provides average daily and monthly values.

The reach Alagón-Zaragoza was considered in order to observe if the model is able to represent correctly the actual hydrodynamic flow variables of the river, to analyse the longitudinal flow behaviour in a low range of 20–50 m^3/s and to verify the sensitivity of the temperature in front of these flows.

The discharges are low in this period, because it is a summer period with almost no rainfall, and there is an average discharge derivation of 20–50 m^3/s approximately towards an adjacent irrigation canal. This canal runs parallel to the Ebro river, by its right margin along about 108 km. The surface irrigated by this canal is 26.500 Ha.

A contribution of flow to be considered in this section is from the Jalón river. This tributary is located 13 km downstream the Alagón station. Both the flow equations and the water temperature equation were included in the model.

The comparison of the measured and simulated time evolution of the water temperature at the downstream section located at Zaragoza in that period is shown in Figure 10. The blue line corresponds to the temperature evolution obtained using the raw daily average meteorological data available. The difference between the numerical and measured temperature can be due to an error in the measurement equipment as well as to the temporal variation in the meteorological variables throughout the day that was not properly recorded. Therefore, a calibration is necessary to obtain satisfactory results. The solar radiation and the average air temperature were adjusted over the daily average in order to generate a reasonable hourly variation (see Table 5), whereas the wind speed (3.11 m/s) and the relative humidity (0.45) were assumed constant. The calibration process consisted of performing trial and error simulations until reaching a set of parameters that adequately fit the measured and simulated values. The minimum values of solar radiation and air temperature are 50 cal/cm^{2}d and 20 °C, respectively. The reason is that heat exchange is also determined by wind speed and relative humidity

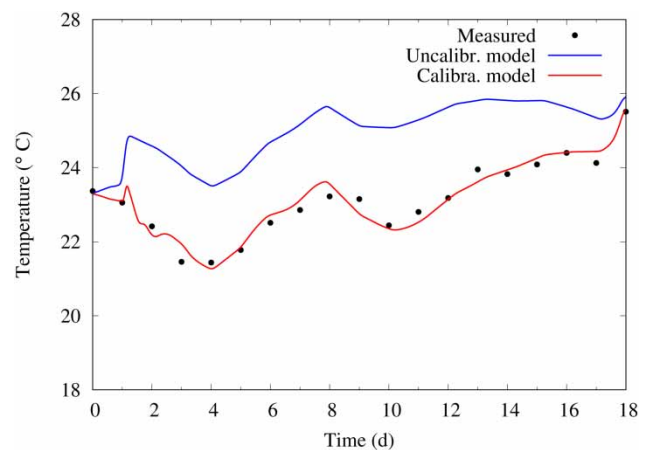**Figure 9** | Location map showing the study reach for Cases 5 and 6.

Figure 10 | Case 5. Comparison of the model with measured data at the Zaragoza station in the Ebro river.

Table 5 | Case 5. Calibrated meteorological variables

Time (h)	Net solar radiation (cal/cm² d⁻¹)	Air temperature (°C)
0	50	20
12	650	32
24	50	20
36	550	28
48	50	20
60	480	30
72	50	20
84	272	25
96	50	20
108	550	28
120	50	20
132	520	30
144	50	20
156	450	27
168	50	20
180	420	28
192	50	20
204	500	25
216	50	20
228	470	29
240	50	20
252	600	32
264	50	20
276	480	32
288	50	20
300	350	29
312	50	20
324	272	30
336	50	20
348	650	26
360	50	20
372	230	29
384	50	20
396	230	28
408	50	20
420	250	29
432	50	20

variations that have been considered as constant in this case. The result after calibration is plotted in Figure 10 (red line).

It is important to emphasize that this data manipulation was only performed when the transported flows were in the range of 20–50 m³/s (Gu & Li 2002).

Concerning the hydraulic variables, the model was run from a dry bed initial condition to the steady state by imposing a constant discharge ($Q = 41$ m³/s) upstream boundary condition and a gauging curve downstream boundary condition. Then, a second run was performed using the actual discharge hydrograph measured by CHE at the upstream section every 15 min. The model responds reasonably well when comparing the time evolution of the flow discharge with respect to the measured data (see Figure 11).
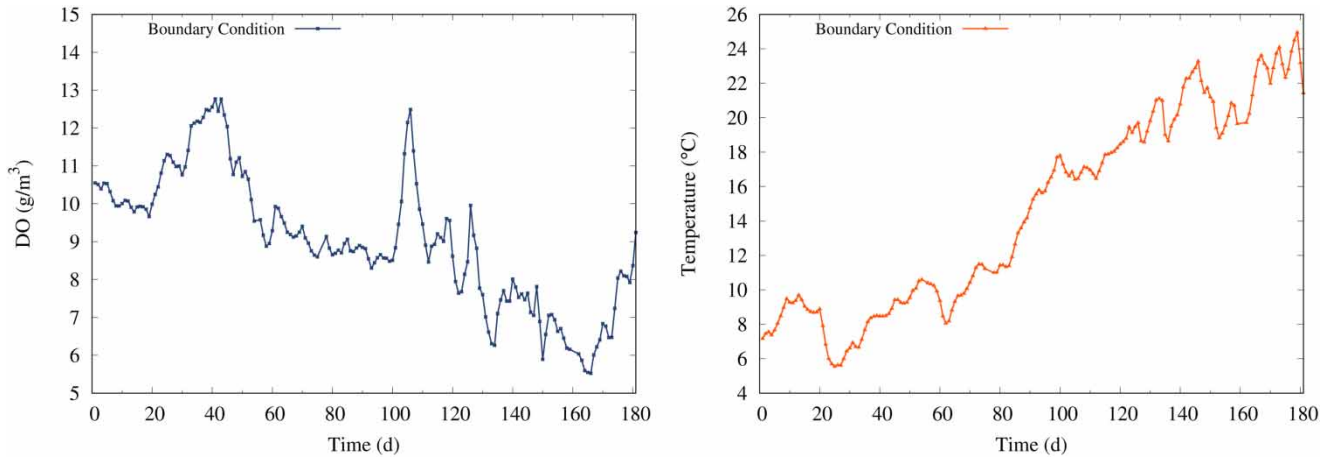
Case 6

The last case is evaluated in the same reach as Case 5, and the interest is focused on the evolution of DO and the temperature under high water discharges and unsteady conditions. There were no data for the rest of the components.

Monitoring stations are located in Alagón, Jalón (at Grisén) and Zaragoza, as shown in Figure 9. The station in Grisén is located approximately 11 km upstream the junction of the tributary Jalón river with the Ebro river.

All gauging stations provide the measurement of discharge, DO and water temperature every 15 min (see Figure 12). The rest of the water quality model components are characterized or directly measured with far less frequency. Therefore, they cannot be used for verification.
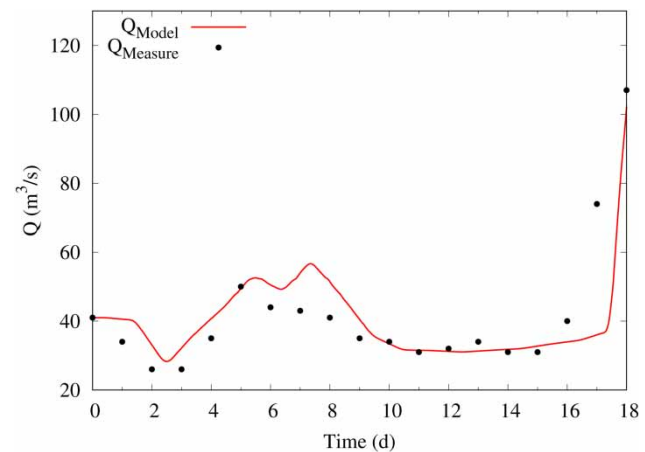
Figure 11 | Case 5. Measured vs. simulated discharge at the Zaragoza station in the Ebro river.

Figure 12 | Case 6. Hourly measure of DO (left) and the water temperature (right) in Alagón.

In order to incorporate them into the full water quality model, initial values were considered zero.

The model was calibrated in the time period from 1 January 2011 to 30 June 2011 (181 days). This process consists in finding the values involved in the considered reaction mechanisms that yield the most accurate simulated results with respect to field measured data.

To begin with the procedure, initial and boundary values are required for both the hydrodynamic variables and the state variables. Conversely, values for the different reaction processes are also required. These values were initially taken from those suggested by Bowie *et al.* (1985) and Ambrose *et al.* (1989). All these values are imposed at the beginning of the simulation. Then, a trial and error process was performed to adjust the measured values with the simulated ones. This verification was carried out at the measurement station located in Zaragoza, both for hydrodynamics and quality.

The parameters obtained from this calibration are shown in Table 6. As can be seen, almost all decay rate and temperature correction factors do not vary too much from the recommended ranges. Therefore, few simulations are necessary to converge to a satisfactory solution.

The numerical solution, presented in Figure 13, depicts the simulated and measured flow-rate variation, while Figure 14 represents the water surface level variation. The flow discharge ranges between 57 and 1,087 m^3/s. This period was chosen to check the efficiency and robustness of the method in the unsteady case due to the strong

Table 6 | Case 6. Calibrated values

Parameter	Unit	Calibrated value	Recommended value
Carbonaceous deoxygenation rate (k_d) at 20 °C	d^{-1}	0.2	0.16–0.21
Half-saturation for carbonaceous (k_{BOD})	gO$_2$/m^3	0.5	0.5
ON mineralization rate (k_{71}) at 20 °C	d^{-1}	0.075	0.075
Nitrification rate (k_{12}) at 20 °C	d^{-1}	0.11	0.09–0.13
Half-saturation for nitrification (k_{NIT})	gO$_2$/m^3	0.5	2.0
Denitrification rate (k_{2d}) at 20 °C	d^{-1}	0.089	0.09
Half-saturation for denitrification (k_{NO_3})	gO$_2$/m^3	0.113	0.1
Oxygen reaeration (θ_R)	–	1.024	1.024
BOD decomposition (θ_{BOD})	–	1.047	1.047
Sediment oxygen demand (θ_{SOD})	–	1.08	1.08
Fraction dissolved CBOD (f_{d5})	–	0.22	0.5
Fraction dissolved ON (f_{d7})	–	1.0	1.0

variations in the flow. Moreover, it included the best and most complete field data set of all the historical data. The results of this scenario provide a reasonable good agreement of the variables flow-rate and water-level surface in the reach under study with a Manning coefficient around 0.035.
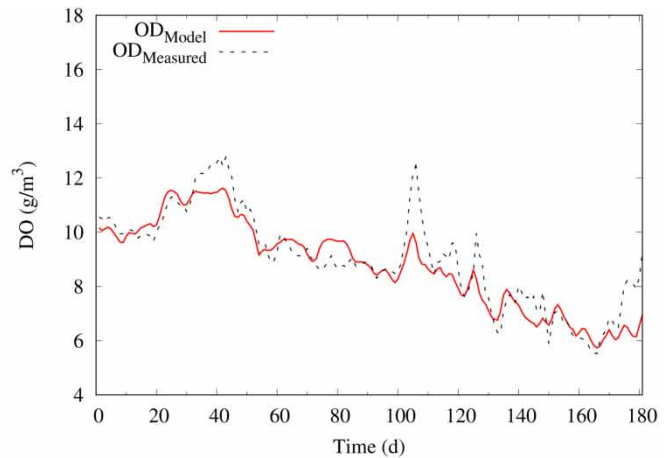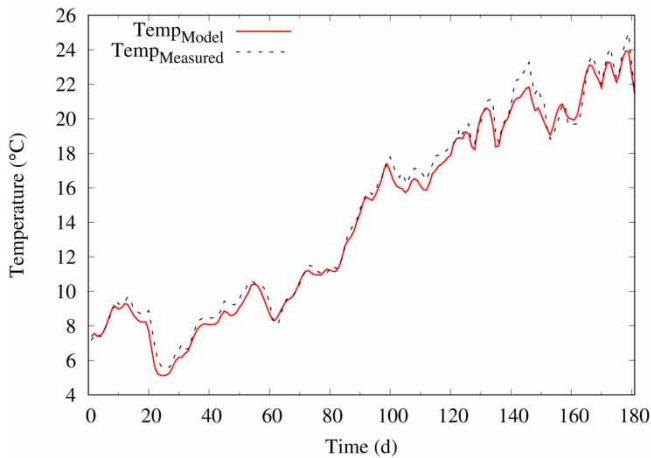
Figure 15 (left) shows the comparison of the numerical temperature predictions with the observed temperature
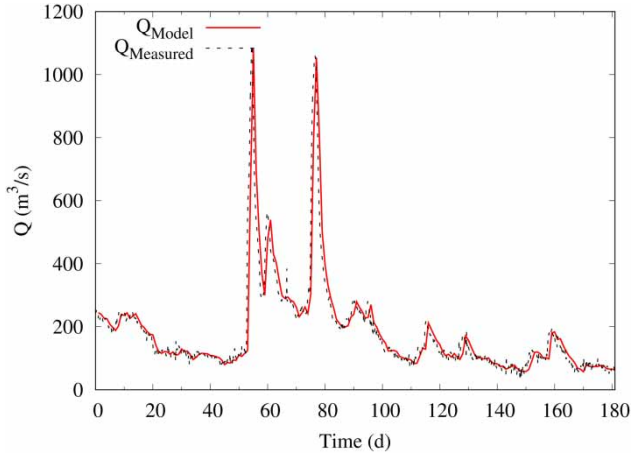
Figure 13 │ Case 6. Measured and simulated flow rate at the Zaragoza station in the Ebro river.
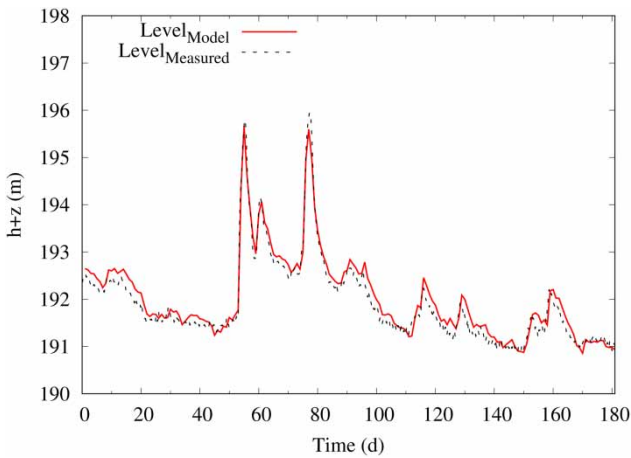
Figure 14 │ Case 6. Time evolution of measured and simulated water level at the Zaragoza station in the Ebro river.

data. It showed a good agreement throughout the simulation period. Conversely, Figure 15 (right) depicts a comparison of the computed and measured DO concentration. Marked differences appeared between observed DO concentrations and those numerically predicted, especially at the concentration peaks. Nevertheless, measured and computed DO concentration distributions showed a reasonably good agreement.

Figure 15 also shows how the increase in the temperature has an effect on the DO concentration. The increase in the temperature on the one hand increases the metabolic rates of aquatic life, at the same time, the available DO is reduced. Thus, as the temperature increases, the oxygen demand increases, while the DO available concentration goes down. If this cycle is prolonged in time it could be harmful, because many organisms would be unable to adapt to the new temperature and therefore disappear.

The longitudinal profile of ammonium was not shown due to its low concentration. Therefore, the concentration of ammonia is also low because of its direct relation with the ammonium.

Analysis of the numerical model

Finally, an analysis of the numerical model was performed with the root mean square error (RMSE) coefficients and Nash–Sutcliffle (N–S) coefficient. The evaluation presented

Figure 15 │ Case 6. Measured and computed water quality values at the Zaragoza station in the Ebro river. Left: Temperature. Right: DO concentration.

in Table 7 shows that in both Cases 3 and 6 for $CBOD_5$ and DO, the adjustment is satisfactory according to the RMSE. For the rest of the proposed cases, the adjustment is very good. Paying attention to the N–S coefficient, the performance of the method is acceptable in Cases 3 and 6 (for the DO variable) and optimal for other cases. The performance indexes for Case 6 can be increased by improving the control over the following issues:

(a) The quality of the available data to calibrate the water quality model was limited. The data required at the boundaries for the state variables considered were not provided at a rate of 15 min as the hydraulic data. The sampling period for some variables of quality is typically characterized by a too low measuring frequency (quarterly). Therefore, the missing information was generated by linear interpolation.

(b) The reaction rates for the different processes were not calibrated *in situ*, only adjusted with the recommended values. These rates may vary depending on the water body, so it is convenient to calibrate *in situ* or in the laboratory.

(c) The quality of the data measured and protocols for the design of data collection at different locations along the river are incomplete. This deficiency is often due to the lack of investment on a suitable monitoring for the quality control stations.

Table 7 | Quantitative analysis of the numerical model

Case	Variable	Coefficient			
		RSME	Fit	N–S	Fit
Case 2	DO	0.0922	v.g.	0.991	o.
	CBOD	0.191	v.g.	0.997	o.
	DO	0.190	v.g.	0.9227	o.
Case 3	$CBOD_5$	0.705	s.	0.676	a.
	NH_3	0.224	v.g.	0.752	a.
	NO_3	0.135	v.g.	0.891	a.
Case 4	T	0.1774	v.g.	0.994	o.
	DO	0.104	v.g.	0.991	o.
Case 5	T	0.241	v.g.	0.943	o.
Case 6	DO	0.689	s.	0.814	a.
	T	0.533	v.g.	0.991	o.

v.g, very good; s, satisfactory; o., optimal; a., acceptable.

CONCLUSIONS

A complete hydrodynamic and water quality model has been presented as a useful numerical tool for the numerical simulation of river water quality and temperature evolution under steady and unsteady conditions. This cross-section averaged model is able to estimate complex temporal scenarios, in each of the physical processes present in real environments. Physical processes, such as kinetic equations, tributaries, abstractions and heat fluxes, are included to model the seasonal evolution of the water depth, discharge, temperature and concentration of several components. The resulting system of equations has been solved using a finite volume formulation that ensures stable and conservative solutions under all flow regimes.

Through calibration and validation, the proposed model is able to represent the reality of the interactions between hydrodynamics and quality accurately and reliably. Therefore, the combined model serves as a predictive tool for water quality in various scenarios. This tool could be useful to the entities providing this service, because it would allow them to reduce and define correctly the location of the quality measurement stations.

A particularity of the model when evaluated during the summer period was the sensitivity of the water temperature to the flows. This sensitivity appears when the transported flow rate is less than 50 m^3/s. The results showed that a careful calibration must be carried out on the daily variation of air temperature and solar radiation. It is worth mentioning that this sensitivity disappears when the transported flows are higher than 50 m^3/s.

In all the proposed scenarios, the response of the model has been satisfactorily evaluated with the field data as well as the literature tests. The temporal distributions of both quality and flow variables in all cases are free of oscillations throughout the period of time under study.

Finally, another characteristic of the model is its usefulness in the academic field, because it allows the comparison of the different processes with known analytical solutions.

The suitable way to apply these alterations allows us to know the real characteristics of the ecosystems, at the same time as it helps us in the analysis of environmental problems. Being able to identify these problems is of vital importance, because they allow us to elaborate

environmental management plans especially when the bodies of water are large and complex.

SUPPLEMENTARY MATERIAL

The Supplementary Material for this paper is available online at https://dx.doi.org/10.2166/hydro.2019.080.

REFERENCES

Ambrose, R. B. & Barnwell, T. O. 1989 Environmental software at the US Environmental Protection Agency's Center for exposure assessment modeling. *Environmental Software* **4** (2), 76–93.

Ambrose, R. B., Wool, T. A. & Martin, J. L. 1993 *The Water Quality Analysis Simulation Program, WASP5, Part A: Model Documentation*. Environmental Research Laboratory, US Environmental Protection Agency, Athens, GA.

Audusse, E., Bouchut, F., Bristeau, M. O., Klein, R. & Bt, P. 2004 A fast and stable well-balanced scheme with hydrostatic reconstruction for shallow water flows. *SIAM Journal on Scientific Computing* **25** (6), 2050–2065.

Bowie, G. L., Mills, W. B., Porcella, D. B., Campbell, C. L., Pagenkopf, J. R., Rupp, G. L., Johnson, K. M., Chan, P., Gherini, S. A. & Chamberlin, C. E. 1985 *Rates, Constants, and Kinetics Formulations in Surface Water Quality Modeling*, 2nd edn. US Environmental Protection Agency, Washington, D.C, EPA/600/3-85/040.

Brown, L. C. & Barnwell, T. O. 1987 *The Enhanced Stream Water Quality Models QUAL2E and QUAL2E-UNCAS: Documentation and User Manual*. US Environmental Protection Agency, Office of Research and Development, Environmental Research Laboratory, Athens, GA.

Brunner, G. W. 2010 *HEC-RAS River Analysis System: Hydraulic Reference Manual*. US Army Corps of Engineers, Institute for Water Resources, Hydrologic Engineering Center, Davis, CA.

Burguete, J. & Garcia-Navarro, P. 2001 Efficient construction of high-resolution TVD conservative schemes for equations with source terms: application to shallow water flows. *International Journal for Numerical Methods in Fluids* **37** (2), 209–248.

Burguete, J., García-Navarro, P. & Murillo, J. 2008 Friction term discretization and limitation to preserve stability and conservation in the 1D shallow-water model: application to unsteady irrigation and river flow. *International Journal for Numerical Methods in Fluids* **58** (4), 403–425.

Cea, L. & Vázquez-Cendón, M. E. 2012 Unstructured finite volume discretisation of bed friction and convective flux in solute transport models linked to the shallow water equations. *Journal of Computational Physics* **231** (8), 3317–3339.

Cea, L., Bermúdez, M., Puertas, J., Blade, E., Corestein, G., Escolano, E., Conde, A., Bockelmann-Evans, B. & Ahmadian, R. 2016 IberWQ: new simulation tool for 2D water quality modelling in rivers and shallow estuaries. *Journal of Hydroinformatics* **18** (5), 816–830.

Chapra, S. C. 2008 *Surface Water-Quality Modeling*. Waveland Press, Long Grove, IL.

Chen, G., Wu, Z. & Zeng, L. 2012 Environmental dispersion in a two-layer wetland: analytical solution by method of concentration moments. *International Journal of Engineering Science* **51**, 272–291.

Cox, B. 2003 A review of currently available in-stream water-quality models and their applicability for simulating dissolved oxygen in lowland rivers. *Science of the Total Environment* **314**, 335–377.

DHI 2009 *Manual. MIKE 11 – A Modeling System for Rivers and Channels*. Danish Hydraulic Institute, Hørsholm.

Di Toro, D. M., O'Connor, D. J. & Thomann, R. V. 1971 A dynamic model of the phytoplankton population in the Sacramento–San Joaquin Delta. In: *Nonequilibrium Systems in Natural Water Chemistry*, chap. 5. Advances in Chemistry, Vol. 106. ACS, Washington, DC, pp. 131–180. doi:10.1021/ba-1971-0106.ch005.

Edinger, J. E., Duttweiler, D. W. & Geyer, J. C. 1968 The response of water temperatures to meteorological conditions. *Water Resources Research* **4** (5), 1137–1143.

Gordillo, G., Morales-Hernández, M. & García-Navarro, P. 2018 A finite volume model for the simulation of water quality in rivers. In: *New Challenges in Hydraulic Research and Engineering*, Vol. 5. (G. Gordillo, M. Morales-Hernandez & P. Garcia-Navarro, eds). International Association for Hydro-Environment Engineering and Research, Trento, Italy.

Gu, R. R. & Li, Y. 2002 River temperature sensitivity to hydraulic and meteorological parameters. *Journal of Environmental Management* **66** (1), 43–56.

Herb, W. R. & Stefan, H. G. 2011 Modified equilibrium temperature models for cold-water streams. *Water Resources Research* **47** (6).

Hirsch, C. 2007 *Numerical Computation of Internal and External Flows: The Fundamentals of Computational Fluid Dynamics*. Elsevier, Amsterdam, The Netherlands.

Huang, J., Yin, H., Chapra, S. C. & Zhou, Q. 2017 Modelling dissolved oxygen depression in an urban river in China. *Water* **9** (7), 520.

Ji, Z. G. 2017 *Hydrodynamics and Water Quality: Modeling Rivers, Lakes, and Estuaries*. John Wiley & Sons, Hoboken, NJ, USA.

Jian, L., Zhongwu, J. & Wenjun, Y. 2014 Numerical modeling of the Xiangxi River algal bloom and sediment-related process in China. *Ecological Informatics* **22**, 23–35.

Kannel, P. R., Kanel, S. R., Lee, S., Lee, Y. S. & Gan, T. Y. 2011 A review of public domain water quality models for simulating dissolved oxygen in rivers and streams. *Environmental Modeling & Assessment* **16** (2), 183–204.

Lee, I., Hwang, H., Lee, J., Yu, N., Yun, J. & Kim, H. 2017 Modeling approach to evaluation of environmental impacts on river water quality: a case study with Galing river, Kuantan, Pahang, Malaysia. *Ecological Modelling* **353**, 167–173.

Liangliang, G. & Daoliang, L. 2015 A review of hydrological/water-quality models. *Frontiers of Agricultural Science and Engineering* **1** (4), 267–276.

Lindenschmidt, K. E. 2006 The effect of complexity on parameter sensitivity and model uncertainty in river water quality modelling. *Ecological Modelling* **190** (1), 72–86.

Morales-Hernández, M., García-Navarro, P. & Murillo, J. 2012 A large time step 1D upwind explicit scheme (cfl > 1): application to shallow water equations. *Journal of Computational Physics* **231** (19), 6532–6557.

Morales-Hernández, M., Murillo, J. & García-Navarro, P. 2018 Diffusion–dispersion numerical discretization for solute transport in 2D transient shallow flows. *Environmental Fluid Mechanics*. doi:10.1007/s10652-018-9644-2.

Murillo, J. & García-Navarro, P. 2010 Weak solutions for partial differential equations with source terms: application to the shallow water equations. *Journal of Computational Physics* **229** (11), 4327–4368.

Murillo, J. & García-Navarro, P. 2012 Wave Riemann description of friction terms in unsteady shallow flows: application to water and mud/debris floods. *Journal of Computational Physics* **231** (4), 1963–2001.

Murillo, J. & Garcia-Navarro, P. 2014 Accurate numerical modeling of 1D flow in channels with arbitrary shape. Application of the energy balanced property. *Journal of Computational Physics* **260**, 222–248. doi:10.1016/j.jcp.2013.12.040.

Murillo, J., Garcia-Navarro, P. & Burguete, J. 2009 Conservative numerical simulation of multi-component transport in two-dimensional unsteady shallow water flow. *Journal of Computational Physics* **228** (15), 5539–5573. doi:10.1016/j.jcp.2009.04.039.

Navas-Montilla, A. & Murillo, J. 2018 2D well-balanced augmented ADER schemes for the shallow water equations with bed elevation and extension to the rotating frame. *Journal of Computational Physics* **372**, 316–348.

O'Connor, D. J. 1961 Oxygen balance of an estuary. *Transactions of the American Society of Civil Engineers* **126** (3), 556–575.

Reichert, P., Borchardt, D., Henze, M., Rauch, W., Shanahan, P., Somlyody, L. & Vanrolleghem, P. A. 2001 *River Water Quality Model no. 1*. IWA Publishing, London.

Streeter, H. W. & Phelps, E. B. 1958 *A Study of the Pollution and Natural Purification of the Ohio River*. Technical Report, US Department of Health, Education, & Welfare, Washington DC, USA.

Thomann, R. V. 1963 Mathematical model for dissolved oxygen. *Journal of the Sanitary Engineering Division* **89** (5), 1–32.

Thomann, R. V. & Mueller, J. A. 1987 *Principles of Surface Water Quality Modeling and Control*. Harper & Row, New York, NY, USA.

Wang, Y. F., Huai, W. X. & Wang, W. J. 2017 Physically sound formula for longitudinal dispersion coefficients of natural rivers. *Journal of Hydrology* **544**, 511–523.

Yao, H., Qian, X., Yin, H., Gao, H. & Wang, Y. 2015 Regional risk assessment for point source pollution based on a water quality model of the Taipu River, China. *Risk Analysis* **35** (2), 265–277.